J. Fluid Mech. (1970), *vol.* 40, *part* 3, *pp.* 577–594
Printed in Great Britain

A wake source model for bluff body potential flow

By G. V. PARKINSON AND T. JANDALI
Department of Mechanical Engineering, University of British Columbia

(Received 4 August 1969)

A theory is presented for two-dimensional incompressible potential flow external to a symmetrical bluff body and its wake. The desired flow-separation points are made the critical points of a conformal transformation to a complex plane in which surface sources in the wake create stagnation conditions at the critical points. The stagnation streamlines then transform to tangential separation streamlines in the physical plane, with separation at the desired pressure. The position and strength of the sources are determined by the requirements of separation position and pressure coefficient. The flow inside the separation streamlines is ignored and base pressure is assumed constant at the separation value. Features of the theoretical model include a finite wake width, a pressure distribution on the separation streamlines decreasing asymptotically towards the free stream value at infinity and a simple analytic expression for the pressure distribution on the body. Comparisons of the theory with experimental data and with other theories are presented for the normal plate, the circular cylinder, the 90° wedge, and the elliptical cylinder. Although simpler to apply than the other theories, the present theory produces at least as good agreement with the experimental data.

1. Introduction

To date there are no theories which can predict or describe all of the important features of flows past bodies whose shapes cause flow separation and the formation of a broad wake. The reasons lie in the complexity of the wake dynamics, including the formation of organized vortex systems, and in the lack of knowledge of the link between wake and separation conditions. As a result, theoretical models of such flows include some empiricism.

Flows normal to long bodies of constant bluff cross-section are of considerable interest and importance, and several empirical facts about them are relevant to the creation of theoretical models. First, if the incident flow is uniform, the time-averaged flow quantities, such as velocity and surface pressure distribution, are reasonably two-dimensional except near the ends of the body span. Secondly, the separating shear layers are thin and well-defined close to the body, and the flow external to these shear layers and to the thin boundary layer on the body surface upstream of separation is irrotational. Thirdly, the time-averaged base pressure over the body surface exposed to the wake is nearly constant for most shapes. This base pressure is always lower than the free-stream pressure.

These facts suggest the use of a two-dimensional irrotational flow model, conveniently treated in the complex plane, to represent time-averaged flow conditions near the body, and particularly its surface loading. Previous models meeting these criteria have employed hodograph methods, in which the separation shear layers are replaced by free streamlines bounding the external irrotational flow. The position of these streamlines is initially unknown but the velocity along them is specified in magnitude and/or direction, and, with the usual inviscid boundary condition on the body surface upstream of separation, the external flow problem is completely specified and can be solved using conformal transformations of the complex velocity and the complex potential planes, with the complex potential as fundamental independent variable. These models do not involve the space actually occupied by the wake, and it is assumed that the body surface exposed to the wake is at the constant base pressure given by the separation value. Two examples of this class of theories which have proved useful and realistic were developed by Roshko (1954) and Woods (1955). In the present theory complex variable methods are used differently.

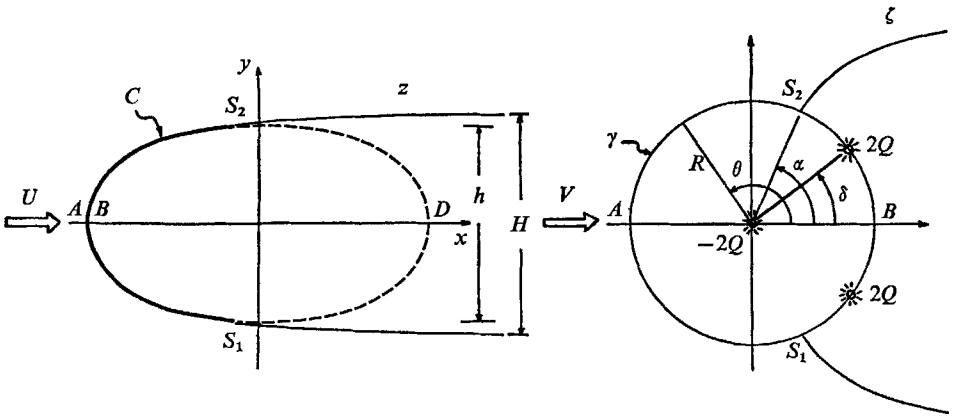

FIGURE 1. Physical and basic transform planes.

2. General theory

Consider two-dimensional, incompressible, irrotational steady flow, uniform at infinity, past a body symmetrical with respect to the incident flow, and with symmetrical separation at points S_1, S_2 shown in figure 1, in the z-plane. The upstream part S_1AS_2 of the body contour C is mapped conformally from the corresponding part of a circle γ in the ζ-plane by the analytic function,

$$z = f(\zeta), \tag{2.1}$$

which preserves the direction, but not necessarily the magnitude, of the velocity at infinity, and for which the points S_1, S_2 are critical points, at which the derivative $f'(\zeta)$ has simple zeros. Accordingly, angles of intersection of curves are doubled at S_1, S_2 in the z-plane and the complete circle γ is mapped onto the slit

$S_1AS_2BS_1$. The part of the actual body contour C downstream of separation S_2DS_1 lies in the wake and is ignored.

In the ζ-plane, the basic flow past the circle γ is the familiar combination of uniform flow in the direction of the real axis plus flow from a suitable doublet at the origin. To this is added the flow from surface double sources of strength $2Q$ symmetrically located at angles $\pm\delta$ on the contour γ, and from their image sinks at the origin. (The combination of a double source on the circle and a sink at the centre satisfies the boundary condition on the circle. It is the limiting case of the combination of a source outside the circle and its image source and sink inside.) The complex potential of the resulting flow is

$$F(\zeta) = V\left(\zeta+\frac{R^2}{\zeta}\right)+\frac{Q}{\pi}[\ln(\zeta-Re^{i\delta})+\ln(\zeta-Re^{-i\delta})-\ln\zeta], \tag{2.2}$$

and the complex velocity in the ζ-plane is

$$w(\zeta) = \frac{dF}{d\zeta} = V\left(1-\frac{R^2}{\zeta^2}\right)+\frac{Q}{\pi}\left[\frac{1}{\zeta-Re^{i\delta}}+\frac{1}{\zeta-Re^{-i\delta}}-\frac{1}{\zeta}\right]. \tag{2.3}$$

The upstream flow from the surface sources creates symmetrical surface stagnation points and these are located at S_1 and S_2 by setting $w(\zeta) = 0$ there, from which a relation between Q and δ is obtained. Because of the doubling of angles at the critical points, the stagnation streamlines leaving S_1 and S_2 in the ζ-plane become tangential separation streamlines at S_1 and S_2 in the z-plane. Separation is assumed to occur at the empirically given base pressure p_b, and this determines the complex velocity in the z-plane at S_1 and S_2, through Bernoulli's equation,

$$p+\tfrac{1}{2}\rho|w(z)|^2 = p_\infty+\tfrac{1}{2}\rho U^2,$$

or

$$C_p = \frac{p-p_\infty}{\frac{1}{2}\rho U^2} = 1-\frac{|w(z)|^2}{U^2}, \tag{2.4}$$

where C_p is the pressure coefficient. With the complex potentials equated at corresponding points of the z- and ζ-planes, complex velocity $w(z)$ is given in terms of $w(\zeta)$ by

$$w(z) = \frac{w(\zeta)}{f'(\zeta)}, \tag{2.5}$$

and, since both $w(\zeta)$ and $f'(\zeta)$ have simple zeros at S_1 and S_2, $w(z)$ is finite there and is equated to the value given by

$$\frac{|w(z)|}{U} = k = (1-C_{p_b})^{\frac{1}{2}}. \tag{2.6}$$

This gives a second relation between Q and δ, which are thereby determined. The surface pressure distribution over the upstream surface S_1AS_2 can now be determined from (2.1), (2.5), and (2.4). The flow inside the separation streamlines is ignored and the pressure over the downstream surface, S_2DS_1 is assumed constant at p_b. The drag D is given by direct integration,

$$D = 2\int_0^{\frac{1}{2}h}(p-p_b)\,dy,$$

or, in terms of the drag coefficient,

$$C_d = \frac{D}{\frac{1}{2}\rho U^2 h} = \frac{2}{h}\int_0^{\frac{1}{2}h} (C_p - C_{p_b})\, dy. \tag{2.7}$$

The shape of the separation streamlines is given by solving for the ζ co-ordinates satisfying

$$\mathrm{Im}\,[F(\zeta)] = \pm Q, \tag{2.8}$$

and then using (2.1) to find the corresponding z co-ordinates. The pressure distribution along these streamlines is then found from (2.5) and (2.4). The asymptotic downstream spacing H of the separation streamlines is given by the continuity equation for the flow from the surface sources

$$2Q = UH. \tag{2.9}$$

In the following sections of the paper, some examples are worked out and compared with other theoretical and with experimental results.

3. Normal flat plate

The normal flat plate shown in figure 2 is mapped from the circle γ in the ζ-plane of figure 1 by the Joukowsky transformation

$$z = f(\zeta) = \zeta - R^2/\zeta, \tag{3.1}$$

where

$$R = \tfrac{1}{4}h,$$

and, since separation occurs at the edges of the plate,

$$\alpha = \tfrac{1}{2}\pi.$$

Since $f'(\zeta) = 1$ at infinity, $V = U$, and $w(\zeta)$ on γ is given from (2.3) by

$$w(\zeta) = 2ie^{-i\theta}\left[U\sin\theta + \frac{Q}{4\pi R}\left(\cot\frac{\delta-\theta}{2} - \cot\frac{\delta+\theta}{2}\right)\right]. \tag{3.2}$$

Equating (3.2) to zero for $\theta = \pm\frac{1}{2}\pi$ gives

$$Q = \tfrac{1}{2}\pi U h\cos\delta. \tag{3.3}$$

It is convenient to express $w(z)$ on C in terms of the parametric variable, θ, so that

$$\frac{w(z)}{U} = \frac{i}{\cos\theta}\left[\sin\theta + \tfrac{1}{2}\cos\delta\left(\cot\frac{\delta-\theta}{2} - \cot\frac{\delta+\theta}{2}\right)\right] = \frac{-i\sin\theta}{\cos\delta - \cos\theta}, \tag{3.4}$$

after some rearrangement, which eliminates the indeterminacy at $\theta = \pm\frac{1}{2}\pi$. As a result, (2.6) gives

$$\sec\delta = k. \tag{3.5}$$

The pressure distribution on the front of the plate is given from (2.4), (3.4) and (3.1), by

$$\left.\begin{aligned} C_p(\theta) &= 1 - \frac{\sin^2\theta}{(\cos\delta - \cos\theta)^2}, \\ y &= \tfrac{1}{2}h\sin\theta, \end{aligned}\right\} \tag{3.6}$$

and C_d is given by (2.7),

$$C_d = 3 - \pi\cos\delta + \frac{\cos 2\delta}{\sin\delta}\ln\left[\frac{1+\cos\delta+\sin\delta}{1+\cos\delta-\sin\delta}\right] + \tan^2\delta. \tag{3.7}$$

(2.8) is transcendental and the co-ordinates of the separation streamlines are found from it by trial, after which the variation of C_p along these streamlines is found using (2.3), (2.5) and (2.4). The asymptotic downstream spacing of the separation streamlines is given from (2.9), (3.3), and (3.5) as

$$H = (\pi/k)\,h. \tag{3.8}$$

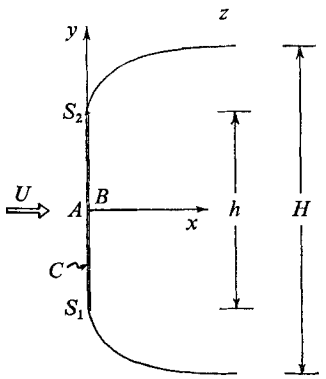

FIGURE 2. Normal flat plate.

Figures 3, 4 and 5 show a comparison, for the same C_{p_b}, of values calculated from the above equations with values given by the notched hodograph theory of Roshko (1954) and experiments of Fage & Johansen (1927). In figure 3, the two theoretical curves for C_p are indistinguishable and their agreement with the experimental points is good. The three values of C_d agreed to within 0·3 %. In figure 4 the two theoretical separation streamlines lie quite close together near the plate, and both are near the middle of the experimentally determined shear layers. However, the asymptotic downstream spacing H given by the present theory is appreciably larger than the constant spacing given by Roshko's theory. In figure 5, all three C_p variations show a similar trend from C_{p_b} at the plate to zero far downstream, but the theoretical curves approach zero more rapidly. It should be noted that the experimental values of figures 4 and 5 are time averages of strongly periodic phenomena, because of the wake vortex formation.

4. Circular cylinder

4.1. *Surface loading and streamline shape*

For the circular cylinder of figure 6, the part of the surface S_1AS_2 upstream of the separation points is mapped as part of the circular arc slit $S_1AS_2BS_1$ from

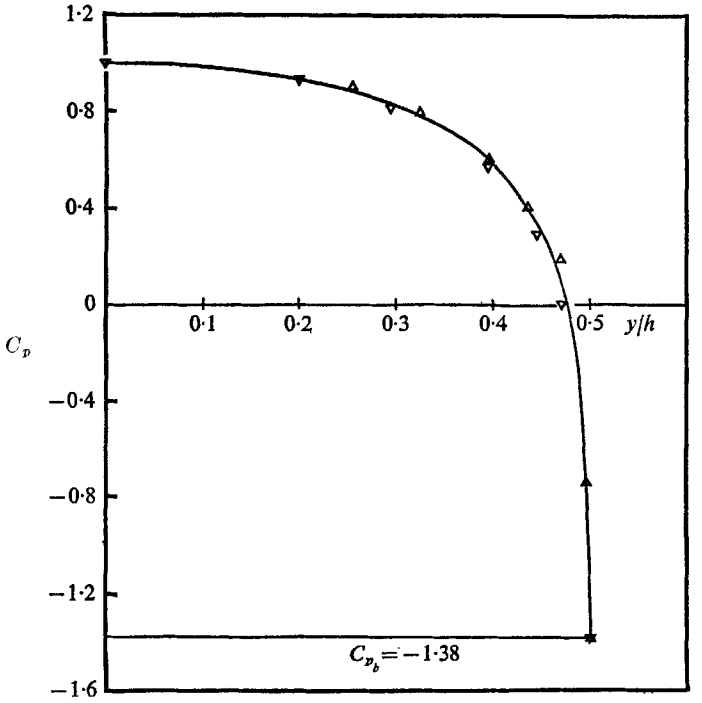

FIGURE 3. Pressure distributions on normal flat plate. ——, present theory, $C_d = 2{\cdot}134$. – – – –, Roshko (1954) theory, $C_d = 2{\cdot}128$. △, ▽, Fage & Johansen (1927) experiments, $C_d = 2{\cdot}13$.

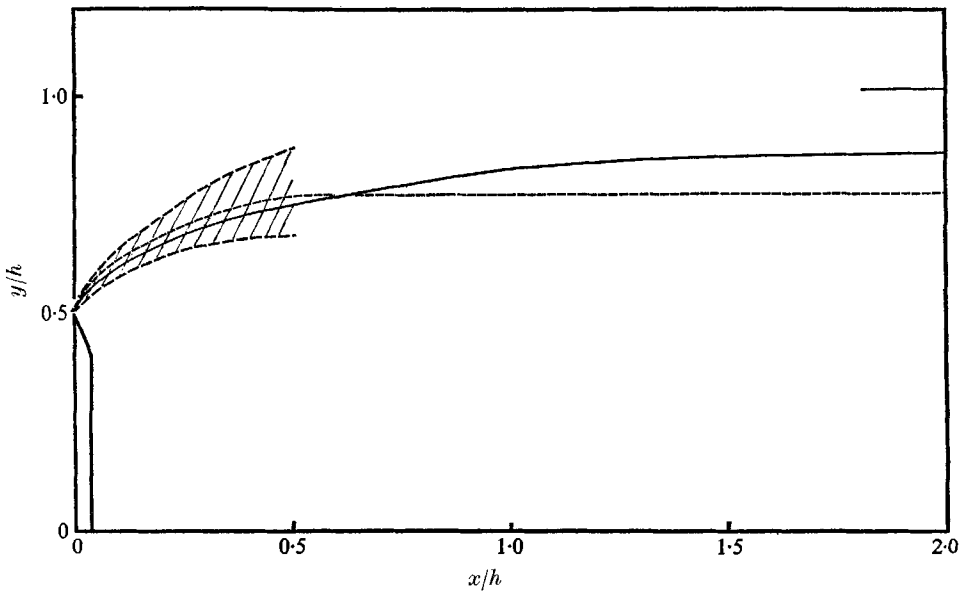

FIGURE 4. Separation streamline shapes for normal flat plate. ——, present theory, – – – –, Roshko (1954) theory. ▨, Fage & Johansen (1927) shear layer measurements.

the circle in the ζ-plane of figure 1 by the transformation,

$$z = f(\zeta) = \zeta - \cot\alpha - \frac{1}{\zeta - \cot\alpha}, \tag{4.1}$$

where the radius of the circle in the ζ-plane is taken to be

$$R = \csc\alpha,$$

and angle α in the ζ-plane is related to the separation angle β_s in the z-plane, assumed known empirically, by

$$\alpha = \tfrac{1}{2}(\pi - \beta_s). \tag{4.2}$$

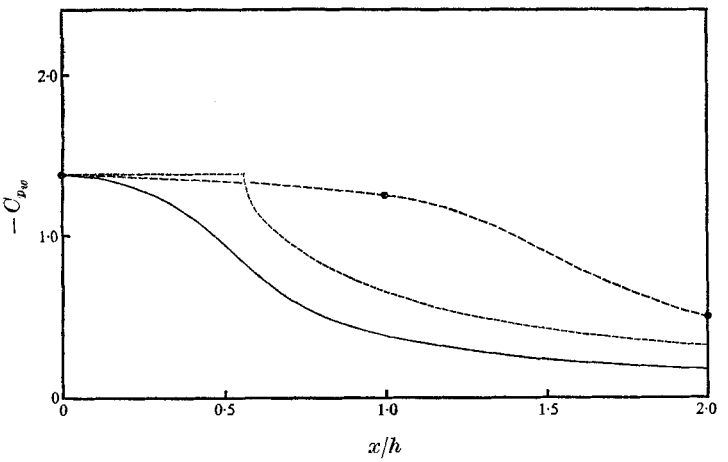

FIGURE 5. Pressure distribution on separation streamlines for normal flat plate. ——, present theory. - - - -, Roshko (1954) theory. – ● –, Fage & Johansen (1927) experiments.

The diameter of the circular cylinder is given by

$$h = 4\csc\beta_s. \tag{4.3}$$

Since $f'(\zeta) = 1$ at infinity, $V = U$ as in the previous case, and $w(\zeta)$ on γ is given again by (3.2). Here, however, (3.2) is equated to zero for $\theta = \pm\alpha$, with the result that

$$Q = 2\pi U \csc\alpha(\cos\delta - \cos\alpha). \tag{4.4}$$

Again, $w(z)$ on C is conveniently expressed in terms of θ as parametric variable, so that, with $dz/d\zeta$ on C given by

$$f'(\zeta) = 1 + \frac{\sin^2\alpha}{(e^{i\theta} - \cos\alpha)^2},$$

the magnitude of the surface velocity over S_1AS_2 is given, after some trigonometric manipulation, by

$$\frac{|w(z)|}{U} = \frac{1}{|f'(\zeta)|}\frac{|w(\zeta)|}{U} = \frac{\sin\theta(1 - 2\cos\alpha\cos\theta + \cos^2\alpha)}{\cos\delta - \cos\theta}. \tag{4.5}$$

Again, the indeterminacy at $\theta = \pm\alpha$ has been eliminated by the rearrangement of terms, and (2.6) gives

$$\cos\delta = \cos\alpha + \frac{\sin^3\alpha}{k}. \tag{4.6}$$

The pressure distribution over S_1AS_2 on C is given by substituting (4.5) in (2.4), and the angular position β on C corresponding to θ on γ is given from (4.1) by

$$\sin\beta = \cos\alpha\left[\frac{\sec\alpha - \cos\theta}{\frac{1}{2}(\sec\alpha + \cos\alpha) - \cos\theta}\right]\sin\theta. \tag{4.7}$$

C_d is determined from (2.7) using (4.5) and (4.7) since

$$y = \tfrac{1}{2}h\sin\beta.$$

The integration is routine but lengthy, and the result is

$$C_d = (1 - C_{p_b} + E)\sin\beta_s + [G\ln J - L(\pi + \beta_s)]\sin\tfrac{1}{2}\beta_s, \tag{4.8}$$

where

$$E = \frac{1}{3(\mu-\nu)}[24\nu^2\mu^3 - 6\nu(3+5\nu^2)\mu^2 + (6+13\nu^2+5\nu^4)\mu - \nu(6-5\nu^2-\nu^4)],$$

$$G = \frac{2}{(1-\mu^2)^{\frac{1}{2}}}[8\nu^2\mu^4 - 6\nu(1+\nu^2)\mu^3 + 2(1-2\nu^2)\mu^2 + \nu(3+5\nu^2)\mu - (1+\nu^2)],$$

$$J = \left[\frac{((1+\mu)(1-\nu))^{\frac{1}{2}} + ((1-\mu)(1+\nu))^{\frac{1}{2}}}{((1+\mu)(1-\nu))^{\frac{1}{2}} - ((1-\mu)(1+\nu))^{\frac{1}{2}}}\right],$$

$$L = 2[4\nu^2\mu^3 - 3\nu(1+\nu^2)\mu^2 + \mu + \nu^3],$$

and

$$\mu = \cos\delta, \quad \nu = \sin\tfrac{1}{2}\beta_s.$$

The co-ordinates of the separation streamlines are found as in the previous case from (2.8). Their asymptotic downstream separation is given from (2.9), (4.2), (4.3), (4.4) and (4.6) as

$$H = (\pi/2k)\sin\beta_s(1+\cos\beta_s)\,h. \tag{4.9}$$

4.2. *Conditions at separation*

Before comparing the present theory with other theories and with experiment it may be useful to examine conditions at separation more closely. The separation angle β_s and the base pressure coefficient C_{p_b} were specified empirically and, while the theory gives separating streamlines which are tangent to the cylinder surface at separation, there is no specification of their curvature there. Knowledge of the curvature is important because of the possibility of physically inadmissible solutions in which the predicted streamlines intersect the cylinder surface downstream of separation.

Information on streamline curvature just after separation can be obtained readily by examining $\partial C_p/\partial\beta$ on the wetted cylinder surface near S_2 (for a general discussion see Woods 1961, §11.6). On S_1AS_2, C_p and β are both functions of θ, so that

$$\left.\frac{\partial C_p}{\partial\beta}\right|_{S_2} = \frac{dC_p/d\theta|_{S_2}}{d\beta/d\theta|_{S_2}} = -2k\frac{(d/d\theta)(|w(z)|/U)|_{S_2}}{d\beta/d\theta|_{S_2}}. \tag{4.10}$$

From (4.7) it is easily shown that $d\beta/d\theta$ is negative on S_1AS_2 and

$$\left.\frac{d\beta}{d\theta}\right|_{S_2} = 0, \tag{4.11}$$

while, from (4.5),
$$\frac{d}{d\theta}\frac{|w(z)|}{U}\bigg|_{S_2} = -k\sec^2\tfrac{1}{2}\beta_s(k-\tfrac{3}{2}\sin\beta_s). \tag{4.12}$$

It follows that $\dfrac{\partial C_p}{d\beta}\bigg|_{S_2}$ is $\begin{cases}\text{positive infinite}, & k<\frac{3}{2}\sin\beta_s,\\ \text{finite}, & k=\frac{3}{2}\sin\beta_s,\\ \text{negative infinite}, & k>\frac{3}{2}\sin\beta_s.\end{cases}$

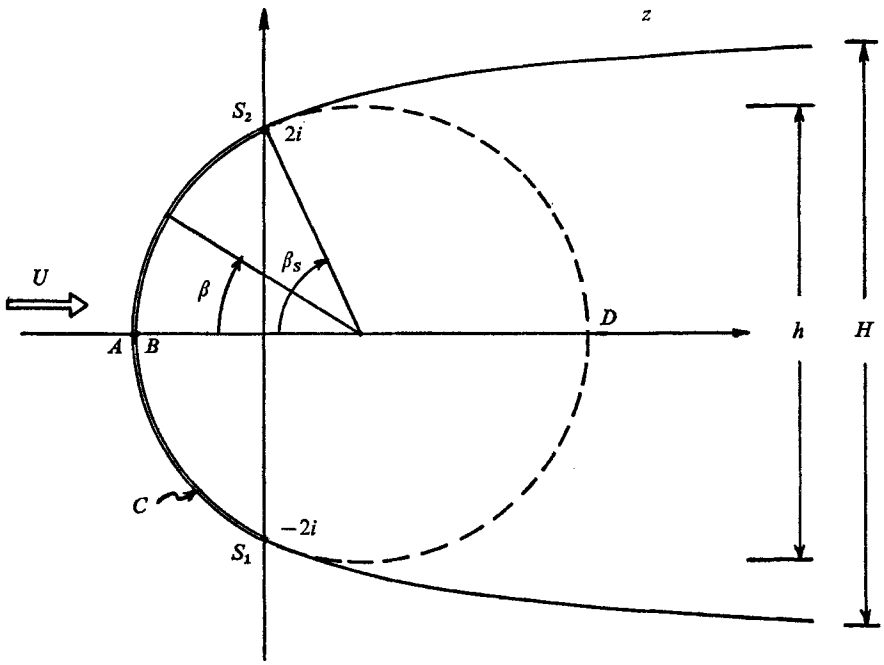

FIGURE 6. Circular cylinder.

The finite value can be found by applying L'Hospital's rule to (4.10), with the result
$$\left.\begin{aligned}\frac{\partial C_p}{\partial\beta}\bigg|_{S_2} &= 3k[1-(4-(\tfrac{4}{3}k)^2)^{\frac{1}{2}}],\\ \sin\beta_s &= \tfrac{2}{3}k.\end{aligned}\right\} \tag{4.13}$$

If $\partial C_p/\partial\beta|_{S_2}$ is negative infinite, it can be shown (see Woods 1961, §11.6) that the separation streamline curvature at S_2 is infinite and convex as viewed from outside the wake, so that the streamline would intersect the cylinder. Thus, any solution with
$$\sin\beta_s < \tfrac{2}{3}k \tag{4.14}$$
is physically inadmissible.

4.3 *Comparisons*

Figures 7, 8, and 9 show comparisons, for the same values of C_{p_b}, of results of the present theory with theoretical results of Roshko (1954) and Woods (1955) and with experimental results of Roshko (1954, 1961) and Bearman (1968).

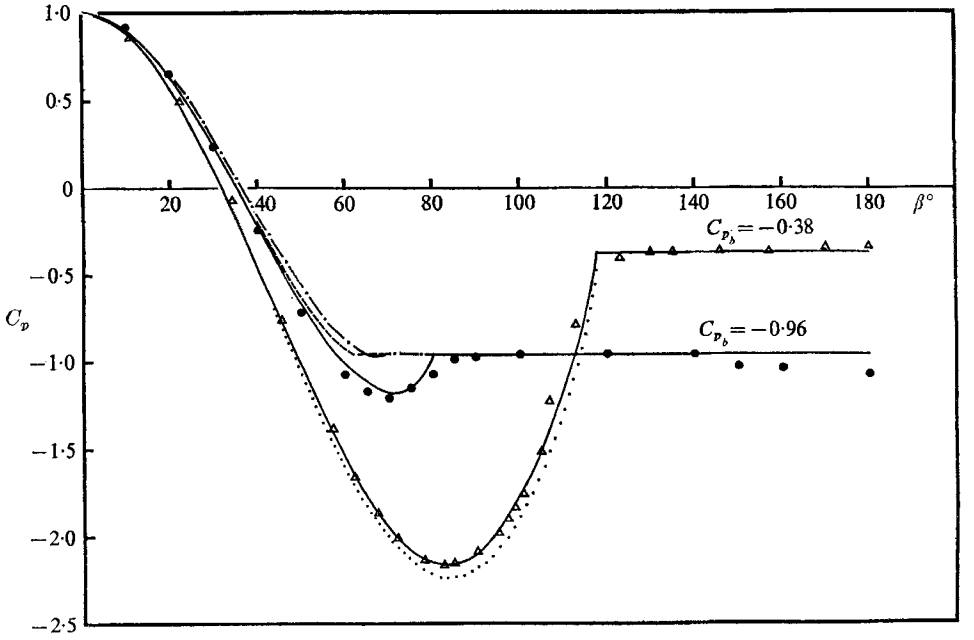

FIGURE 7. Pressure distributions on circular cylinder. ——, present theory. ·——·, present theory with finite curvature condition. – – – –, Roshko (1954) theory. ·····, Woods (1955) theory. ●, Roshko (1954) experiments, Reynolds number 1·45 (10)[4]. △, Bearman (1968) experiments, Reynolds number 2·13(10)[5].

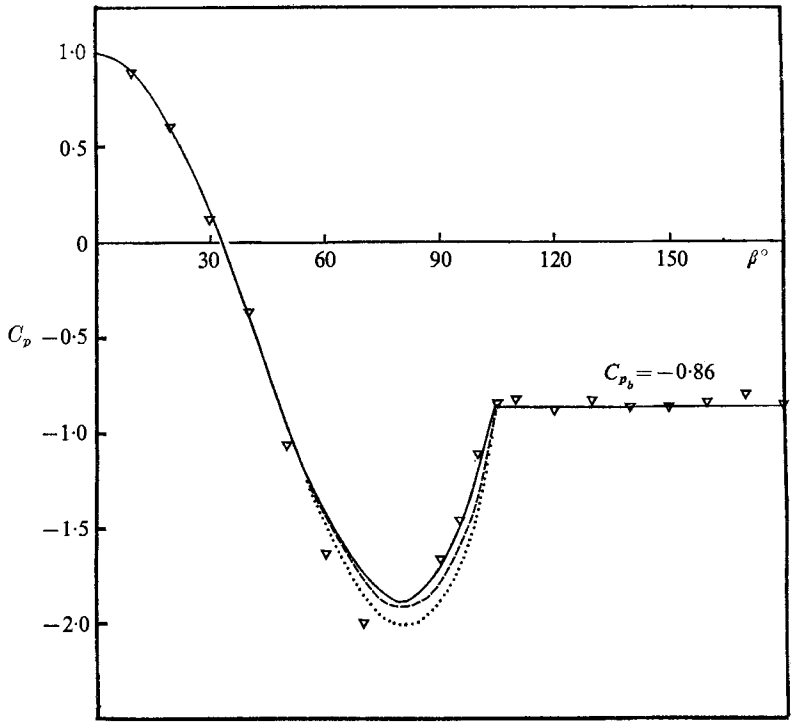

FIGURE 8. Pressure distributions on circular cylinder. ——, present theory. – – – –, Woods (1955) theory, $M = 0$. ·····, Woods (1955) theory, $M = 0·25$. ▽, Roshko (1961) experiments, $M = 0·25$, Reynolds number 8·4(10)[6].

In figure 7, surface pressure distributions are shown for cases representing two values of C_{p_b}. The first of these, $C_{p_b} = -0{\cdot}96$ ($k = 1{\cdot}40$), represents the subcritical Reynolds number range in which laminar separation occurs with $\beta_s \doteq 80°$. The experimental points are from Roshko (1954), and his theoretical curve is also given. His method does not choose β_s empirically, but assumes that the streamline curvature at separation is finite and equal to that of the cylinder, thereby determining β_s as a function of k. For $k = 1{\cdot}40$ this theory gives $\beta_s \doteq 62°$, much less than the experimental value, so that the theoretical curve is inaccurate near separation. The present theory with condition (4.13) applied corresponds to finite streamline curvature at separation, which occurs at $\beta_s = 69{\cdot}0°$, and the pressure distribution so determined is plotted on figure 7. It is seen to agree quite closely with Roshko's curve, and is similarly inaccurate near the actual separation point.

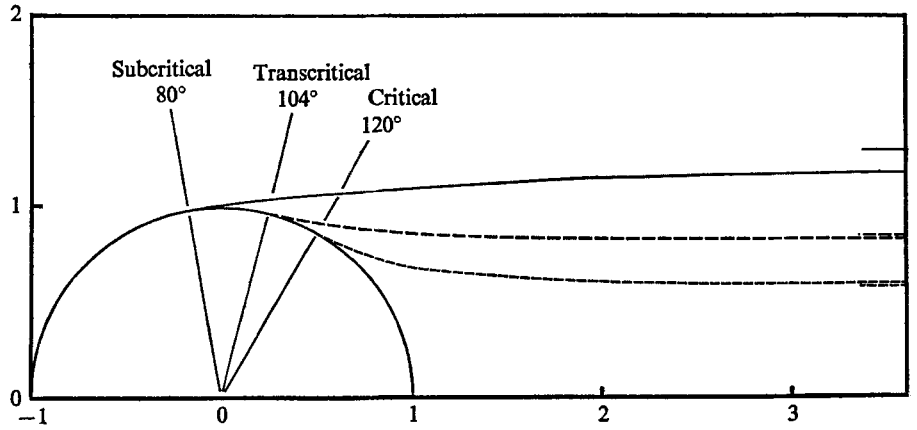

FIGURE 9. Separation streamline shapes for circular cylinder by present theory. ——, $C_{p_b} = -0{\cdot}96$, $C_d = 1{\cdot}09$. – – – –, $C_{p_b} = -0{\cdot}86$, $C_d = 0{\cdot}79$. - - -, $C_{p_b} = -0{\cdot}38$, $C_d = 0{\cdot}34$.

If the finite curvature requirement is abandoned and β_s is chosen empirically as 80°, the present theory gives good agreement with the experimental points. The theory of Woods (1955) was also calculated for this case, and the two theoretical curves are indistinguishable.

The other value of base pressure coefficient, $C_{p_b} = -0{\cdot}38$ ($k = 1{\cdot}175$), represents the critical Reynolds number range in which the usual pressure distribution, in smooth incident flow, is complicated by the presence of laminar separation bubbles. The experimental points presented here, however, were obtained by Bearman (1968) in a turbulent flow produced by upstream grids, and the turbulence appears to have eliminated the bubbles, producing a smooth distribution suitable for the present purpose. The present theory and that of Woods are calculated for $\beta_s = 117{\cdot}5°$ and the plotted curves are seen to be in good agreement with each other and the experimental points. (In comparing the two theories it was useful to choose the same β_s. However, Woods' theory would produce better agreement with the experimental points if β_s were reduced slightly.)

Figure 8 shows pressure distribution for $C_{pb} = -0{\cdot}86$, representing the high transcritical Reynolds number range. The experimental points are from Roshko (1961), and theoretical curves are calculated for $\beta_s = 104°$. The present theory shows good agreement except near the suction peak, which is underestimated. It seemed probable that this discrepancy was caused largely by compressibility effects, since the free stream Mach number M in Roshko's experiment was 0·25.

The present theory is for incompressible flow only, but Woods' theory applies to subsonic flow, and was therefore calculated for both $M = 0$ and $M = 0{\cdot}25$. The two curves for $M = 0$ have the same good agreement as in figure 7, while the curve for $M = 0{\cdot}25$ tends to verify that compressibility effects caused the high experimental suction peak.

Figure 9 gives separation streamline shapes calculated by the present theory for the three types of separation considered in figures 7 and 8. (A slightly different separation angle, $\beta_s = 120°$, was used for the case of critical separation.) It can be seen that the streamlines do not intersect the cylinder surface downstream of separation. In all cases the value of $\partial C_p/\partial\beta|_{S_2}$ is positive infinite, so that (Woods 1961, § 11.6) the curvature of the streamlines at separation is infinite and concave as viewed from outside the wake. This is also true of the examples of Woods' theory presented in figures 7 and 8.

For the three types of separation, drag coefficients calculated by the present theory agreed with measured values within $6\frac{1}{2}\%$. In the next two sections of the paper, the theory is applied, for pressure distribution only, to two other symmetrical shapes.

5. Ninety-degree wedge

For the 90° wedge of figure 10 a different mapping is more useful. The upper half ζ-plane, also shown in figure 10, is mapped on the slit upper half z-plane, with corresponding boundaries NAS_2BN, by the Schwarz–Christoffel transformation

$$dz/d\zeta = f'(\zeta) = K(\zeta+1)^{-\frac{1}{4}}\zeta(\zeta-1)^{-\frac{3}{4}}. \tag{5.1}$$

Only the upper half planes need be considered, by symmetry. (This method could also have been used for the normal flat plate.) (5.1) can be integrated to give

$$z = K\left[(\zeta-1)\left(\frac{\zeta+1}{\zeta-1}\right)^{\frac{3}{4}} + \tanh^{-1}\left(\frac{\zeta+1}{\zeta-1}\right)^{\frac{1}{4}} - \tan^{-1}\left(\frac{\zeta+1}{\zeta-1}\right)^{\frac{1}{4}}\right], \tag{5.2}$$

and the scale factor K is evaluated by setting

$$z = \tfrac{1}{2}h(1+i) \quad \text{for} \quad \zeta = 0,$$

with the result that

$$K = \frac{h}{\ln\cot\frac{1}{8}\pi + \sqrt{2} - \frac{1}{2}\pi}. \tag{5.3}$$

The flow in the upper half z-plane separates at the corner S_2, and, for the flow in the ζ-plane, a double source on the real positive axis at

$$\zeta = \epsilon < 1$$

will permit the location of a stagnation point at S_2. Again, the mapping function

derivative $f'(\zeta)$ has a simple zero at S_2, so the tangential separation condition in the z-plane is satisfied. The complex potential $F(\zeta)$ is given by

$$F(\zeta) = V\zeta + (Q/\pi)\ln(\zeta - \epsilon), \tag{5.4}$$

and the complex velocity

$$w(\zeta) = V + \frac{Q}{\pi}\frac{1}{\zeta - \epsilon}. \tag{5.5}$$

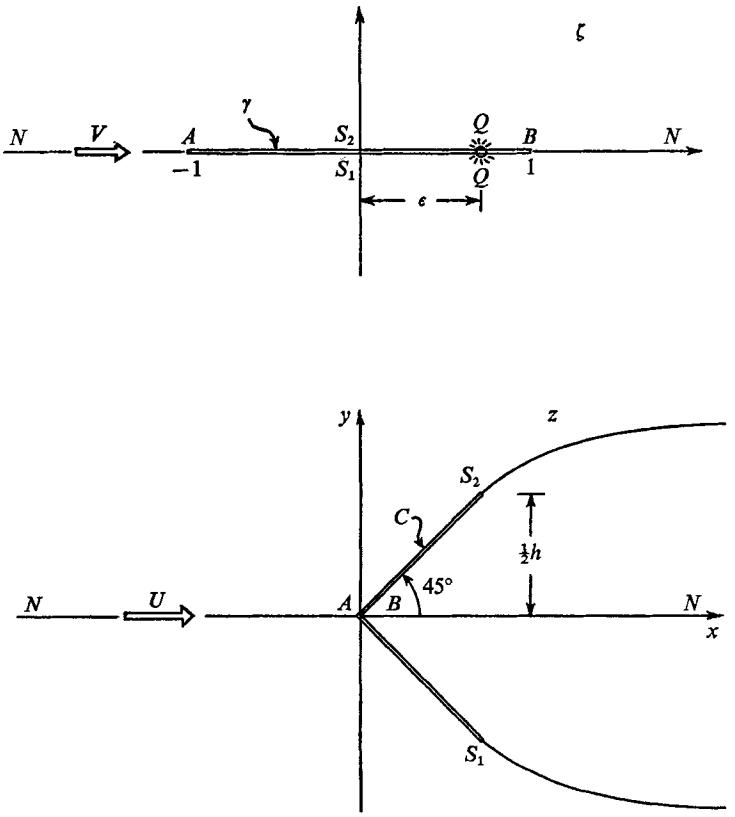

FIGURE 10. 90° wedge and transform plane.

Here $f'(\zeta) = K$ at infinity so that

$$V = KU. \tag{5.6}$$

If (5.5) is equated to zero for $\zeta = 0$,

$$Q = \pi K U \epsilon, \tag{5.7}$$

and, on the wetted surface of the wedge AS_2,

$$\frac{w(z)}{U} = \frac{w(\zeta)}{U}\frac{1}{f'(\zeta)} = \frac{(\zeta+1)^{\frac{1}{2}}(\zeta-1)^{\frac{1}{2}}}{\zeta - \epsilon}. \tag{5.8}$$

Again, the determinacy at $\zeta = 0$ has been eliminated directly, and application of (2.6) gives

$$\epsilon = 1/k. \tag{5.9}$$

By (2.4), (5.8) and (5.9), the pressure distribution on wetted surface AS_2 is given by

$$C_p = 1 - \left| \frac{(\zeta+1)^{\frac{1}{4}}(\zeta-1)^{\frac{3}{4}}}{\zeta-(1/k)} \right|^2 \quad (-1 \leqslant \zeta \leqslant 0),$$

with the corresponding z co-ordinates given by (5.2) and (5.3).

Figure 11 compares, for the same value of C_{p_b}, theoretical C_p-distributions by the present method and that of Roshko (1954) with experimental values by Slater (1969). The two theoretical curves are indistinguishable, and both agree quite closely with the experimental values. It should be noted that the experiments were not actually performed on a wedge, but on a simulated structural angle section 3 in. by 3 in., with legs of rectangular section $\frac{1}{2}$ in. thick, as shown in figure 11.

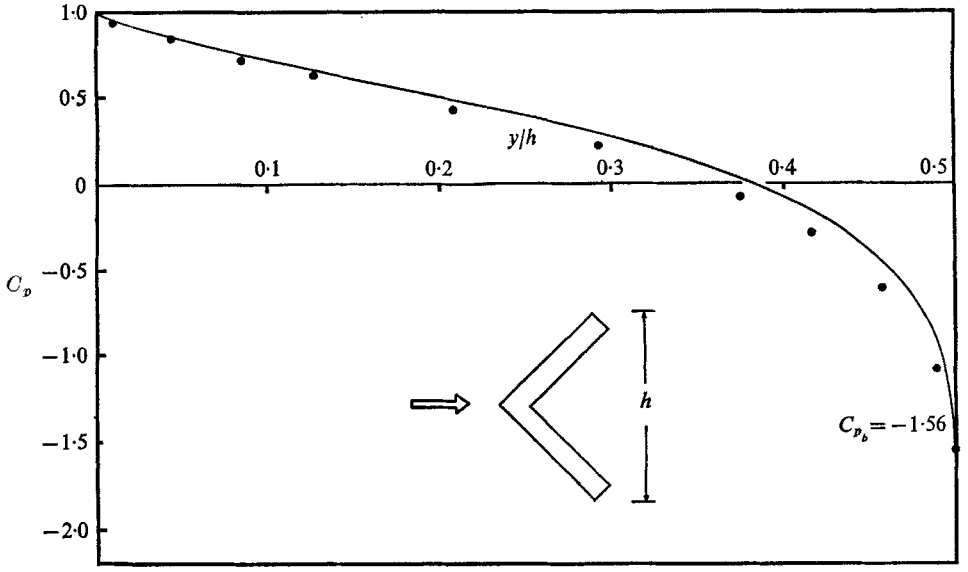

FIGURE 11. Pressure distributions on 90° wedge. ——, present theory. – – – –, Roshko (1954) theory. ●, Slater (1969) experiments.

6. Elliptical cylinder

The elliptical cylinder of eccentricity e^* in the z'-plane of figure 12 is mapped from the circular cylinder in the z-plane of figure 6 by the combination of a Joukowsky transformation, expansion and translation,

$$z' = r'(\tfrac{1}{2}z\sin\beta_s - \cos\beta_s) + \frac{1}{r'(\frac{1}{2}z\sin\beta_s - \cos\beta_s)}, \tag{6.1}$$

where

$$r' = \frac{1}{e^*} + \left(\frac{1}{e^{*2}} - 1\right)^{\frac{1}{2}}.$$

Since S_1, S_2 are not critical points of (6.1), angles are preserved there, and streamlines which leave the circular cylinder in the z-plane tangentially at S_1, S_2

map onto streamlines which leave the elliptical cylinder in the z'-plane tangentially at S_1, S_2. Since the problem for the circular cylinder was solved in § 4, the present problem reduces to choosing the base pressure parameter k in the circular cylinder solution, so that the corresponding parameter for the elliptical cylinder,

$$k' = (1 - C'_{pb})^{\frac{1}{2}},$$

has the correct empirical value. The required relation is obtained from

$$w(z') = \frac{w(z)}{dz'/dz}. \tag{6·2}$$

Since $dz'/dz = \frac{1}{2}r' \sin\beta_s$ at infinity,

$$U' = \frac{U}{\frac{1}{2}r' \sin\beta_s}, \tag{6.3}$$

and
$$\left.\frac{|w(z')|}{U'}\right|_{S_2} = k' = \frac{U}{U'}\frac{|w(z)|/U|_{S_2}}{|dz'/dz||_{S_2}} = \frac{k}{\left|1 - \dfrac{1}{r'^2(\frac{1}{2}z\sin\beta_s - \cos\beta_s)^2}\right|_{S_2}},$$

or
$$k' = k\frac{r'^2}{((r'^2\cos 2\beta_s - 1)^2 + r'^4\sin^2 2\beta_s)^{\frac{1}{2}}}. \tag{6.4}$$

If (6.1) is evaluated for points on S_1AS_2, where

$$z = 2\cot\beta_s + \tfrac{1}{2}h\,e^{i(\pi-\beta)},$$

then
$$z' = -\left(r' + \frac{1}{r'}\right)\cos\beta + i\left(r' - \frac{1}{r'}\right)\sin\beta, \tag{6.5}$$

and, at S_2,
$$\frac{y'_s}{x'_s} = -\tan\beta'_s = -\frac{r' - (1/r')}{r' + (1/r')}\tan\beta_s. \tag{6.6}$$

Also, on S_1AS_2,
$$\frac{|w(z)'|}{U'} = \frac{|w(z)|}{U}\frac{r'^2}{((r'^2\cos 2\beta - 1)^2 + r'^4\sin^2 2\beta)^{\frac{1}{2}}}, \tag{6.7}$$

where $|w(z)|/U$ is given by (4.5), using (4.2), (4.6), and (4.7).

For a given ellipse, r' is known and k' and β'_s are given empirically. β_s and k are then determined from (6·6) and (6·4) and the pressure distribution on the wetted surface of the ellipse can then be found from (6.7) and (6.5).

As for the circular cylinder, the streamline curvature at separation from the elliptical cylinder is important, and again $\partial C_p/\partial\beta'|_{S_2}$ cannot be negative infinite or the streamline will intersect the cylinder. Because of (6.7) and (4.14) this means that solutions with

$$k > \tfrac{3}{2}\sin\beta_s$$

or
$$k' > \frac{3}{2}\frac{r'^2\sin\beta_s}{((r'^2\cos 2\beta_s - 1)^2 + r'^4\sin^2 2\beta_s)^{\frac{1}{2}}} \tag{6.8}$$

are physical inadmissible.

In figure 13 a comparison is made, for an elliptical cylinder of $e^* = 0{\cdot}60$, of two C_p distributions, calculated by the present theory for different assumed

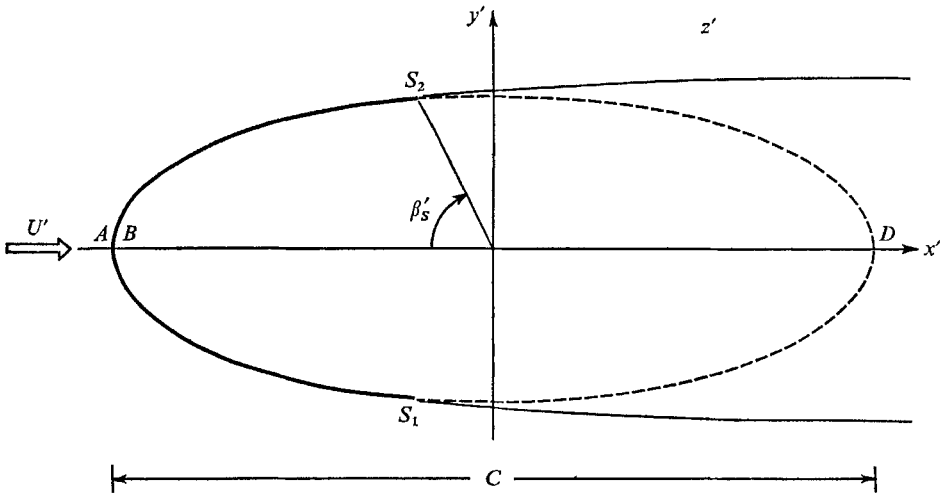

FIGURE 12. Elliptical cylinder.

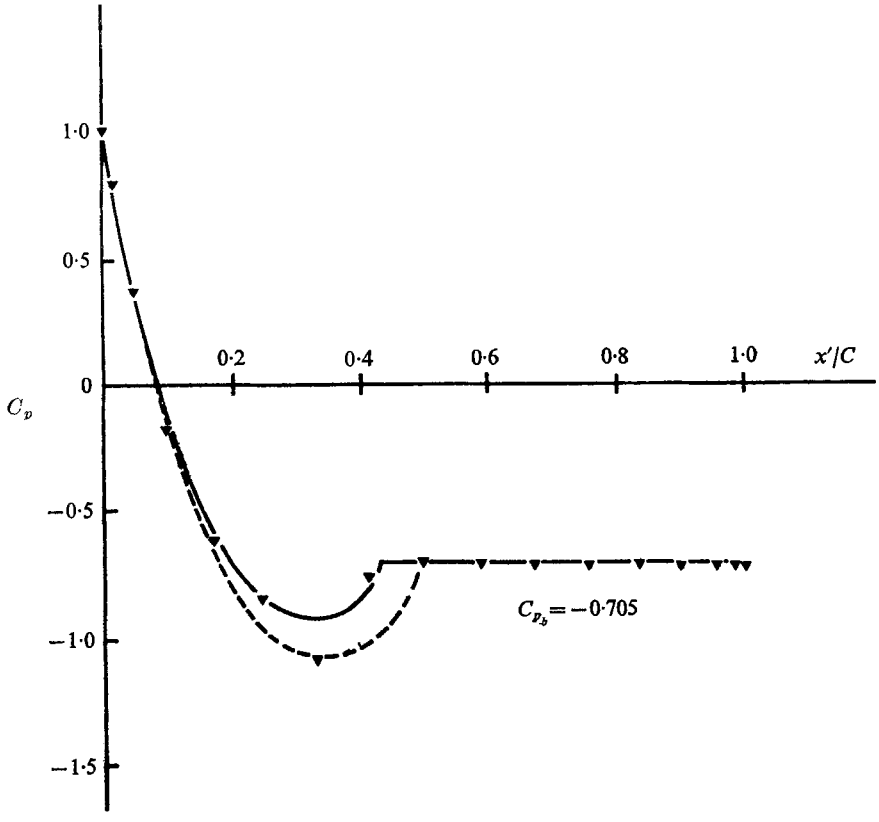

FIGURE 13. Pressure distributions on elliptical cylinder. ——, present theory, $\beta_s' = 80°$. – – – –, present theory, $\beta_s' = 89°$. ▼, Wiland (1968) experiments, Reynolds number 6·8 $(10)^4$.

values of β_s', with experimental values obtained by Wiland (1968). The agreement of the curve for $\beta_s' = 80°$ with the experimental points is good except for one point, which may be a bad point. For this case

$$k' = 1{\cdot}305,$$

and

$$\frac{3}{2}\frac{r'^2 \sin\beta_s}{((r'^2\cos 2\beta_s - 1)^2 + r'^4 \sin^2 2\beta_s)^{\frac{1}{2}}} = 1{\cdot}341,$$

so that although (6.8) is not satisfied, there is not much margin. In fact, when the theory was applied to another elliptical cylinder, with $e^* = 0{\cdot}80$, also tested by Wiland, although k' was less and β_s' about the same, the reduction in r' was large enough that (6.8) was satisfied and the theoretical solution was inadmissible.

7. Concluding remarks

The present theory appears to give at least as good agreement with experiment as other separated potential flow theories, and it has the advantage that it is simpler to use. This advantage is considerable for bodies with curved surfaces, which are less amenable to hodograph methods. For example, Woods' (1955) theory for the circular cylinder requires an iterative, numerical solution of a difficult integral equation. The degree of empiricism in the present theory is the same as in other theories, in that one empirical parameter, the base pressure coefficient, is needed for shapes with separation at convex corners, such as the normal plate, while two parameters, the base pressure coefficient and the separation position are needed for continuous curved shapes, such as the circular cylinder. The criterion of finite streamline curvature at separation, which would link these two parameters for curved shapes, does not appear to lead to realistic results.

The method can readily be extended to other symmetrical shapes whose wetted surfaces can be mapped conformally onto the wetted surface of the circular cylinder of figure 6, as was done for the elliptical cylinder. However, as for the thinner elliptical cylinder mentioned in § 6, the theoretical solutions for relatively thin bodies may prove to be physically inadmissible.

Financial support for this work was obtained from the Canadian National Research Council and Defence Research Board.

REFERENCES

BEARMAN, P. W. 1968 The flow around a circular cylinder in the critical Reynolds number régime. *NPL Aero Report* 1257.

FAGE, A. & JOHANSEN, F. C. 1927 On the flow of air behind an inclined flat plate of infinite span. *Proc. Roy. Soc. Lond.* A **116**, 170.

ROSHKO, A. 1954 A new hodograph for free streamline theory. *NACA TN* 3168.

ROSHKO, A. 1961 Experiments on the flow past a circular cylinder at very high Reynolds number. *J. Fluid Mech.* **10**, 345.

SLATER, J. E. 1969 Aeroelastic instability and aerodynamics of structural angle sections Ph.D. Thesis, University of British Columbia.

WILAND, E. 1968 Unsteady aerodynamics of stationary elliptic cylinders in subcritical flow. M.A.Sc. Thesis, University of British Columbia.

WOODS, L. C. 1955 Two-dimensional flow of a compressible fluid past given curved obstacles with infinite wakes. *Proc. Roy. Soc. Lond.* A **227**, 367.

WOODS, L. C. 1961 *The Theory of Subsonic Plane Flow*. Cambridge University Press.